Vol. 7 No. 2 (2024) 124 – 140 | doi.org/10.33116/ije.v7i2.199

IJE | INDONESIAN JOURNAL OF ENERGY
P-ISSN: 2549-1016 | E-ISSN: 2549-760X
available online at www.ije-pyc.org

Published by: The Purnomo Yusgiantoro Center

Transformation of Lampung Natural Zeolite into Zeolite-A by Aluminium Addition and Application as Catalyst for Biomass Pyrolysis

Syayyidati Aulia [1,*] Wasinton Simanjuntak [1], Kamisah D. Pandiangan [1], Mita Rilyanti [1]

[1] University of Lampung, Jl. Prof. Dr. Ir. Sumantri Brojonegoro No.1, Bandar Lampung, Lampung 35141, Indonesia

*Corresponding Author: syayyidati@gmail.com

Article History

Received 18 October 2023
Accepted 19 August 2024
Available 29 August 2024

Abstract

In this study, the transformed zeolite from Lampung natural zeolite (LNZ) was used as a catalyst for the pyrolysis of a mixture of cassava tubers and rubber seed oil to produce bio crude oil (BCO). Transformation of Lampung natural zeolite into zeolite-A was attempted by adjusting the Si/Al ratios to 1.0, 1.5, and 2.0 transformed with and without aluminum addition and hydrothermal method with variation Si/Al ratio of 1.0; 1.5 and 2.0. The resulting products were specified as Zeo-C, Zeo-R1, Zeo-R1.5 and Zeo-R2.0. XRD analysis results show that Zeo-C and Zeo-R2 were transformed into zeolite-P, while zeolite-A, as targeted, was found in Zeo-R1 and Zeo-R1.5. SEM analysis results were also in accordance with XRD analysis results that showed the bipyramid crystal of zeolite-P in Zeo-C and Zeo-R2, while the cubic crystal of zeolite-A in Zeo-R1 and Zeo-R1.5. The BCO produced by using Zeo-C and Zeo-R1.5 as catalysts has the highest hydrocarbon content of 81% and 98%, respectively. Compared to previous studies, our study introduces an innovative approach by utilizing LNZ, a resource that has not been extensively explored, and combining cassava and rubber seed oil to produce bio-crude oil with a high hydrocarbon content. Our study contributes by promoting the use of underutilized biomass resources, potentially providing an environmentally friendly and economically viable alternative for BCO production.

Keywords:

Lampung natural zeolite, zeolite-A transformation, food grade aluminium foil, biomass pyrolysis, bio crude oil, cassava tubers, rubber seed oil

1. Introduction

According to Government Regulation No. 79 of 2014 on the National Energy Policy, the targets for renewable energy utilization are set at a minimum of 23% by 2025 and 31% by 2050 (Dewan Energi Nasional, 2019). To achieve these ambitious targets, the development of biomass-based renewable energy sources, known as bioenergy, has been pursued nationwide as part of a global initiative. The availability and renewability of various types of biomasses make biofuels a promising solution for replacing conventional fuels such as gasoline and diesel. One significant type of biofuel is bio-oil or bio-crude oil (BCO), which is produced through the pyrolysis of biomass.

Pyrolysis is defined as the process of breaking down large molecules into smaller ones through thermal decomposition. For BCO production, pyrolysis is typically conducted at temperatures ranging from 300 to 500 °C, in an environment devoid of air and with low humidity. This technology offers several advantages, including its applicability to all types of biomasses, the simplicity and speed of the process, and the fact that it does not require expensive equipment (Supriyanto et al., 2018). Furthermore, the fuels produced from pyrolysis can be used for various applications, such as in boilers and turbines, and

can also be upgraded into higher quality fuels, such as bio-gasoline (Simanjuntak et al., 2019). Several types of raw materials have been successfully pyrolyzed, including palm oil (Supriyanto et al., 2018), sugarcane (Iryani et al., 2017), and cassava (Simanjuntak et al., 2019).

Pyrolysis can be conducted with or without a catalyst. Catalyzed pyrolysis is more widely used because catalysts function to accelerate the reaction, reduce the required temperature, and determine the composition of the resulting product (Simanjuntak et al., 2019). One class of catalysts that is particularly attractive for biomass pyrolysis is zeolites due to their ability to enhance deoxygenation in the pyrolysis process. Zeolites are naturally abundant and distributed across various regions. In Indonesia alone, deposits of natural zeolites can be found in more than 50 regions, including Lampung Province. According to the Directorate of Regional Potential Development of the Investment Coordinating Board, the production of natural zeolite in Lampung Province was almost 31.2 million tons in 2012. Natural zeolite possesses good thermal stability properties but has low crystallinity, which results in relatively low catalytic activity (Ngapa et al., 2016). To improve its catalytic activity, one effective method is transforming natural zeolite into synthetic zeolite.

One of the synthetic zeolites that has been widely used is zeolite-A. Due to its various applications, such as in membranes, absorbents, ion exchange, and as a catalyst, zeolite-A has become one of the most attractive materials. It has consistently garnered interest in examining different preparation methods and the utilization of diverse source materials (Simanjuntak et al., 2021). The silicon-to-aluminum (Si/Al) ratio for synthesizing zeolite-A ranges from 1.0 to 1.7 (Mendoza, 2017) and 1.0 to 2.0 (Kristianingrum et al., 2016). Our study used the two biomass feedstocks, which are cassava and rubber seed oil, for several reasons. Cassava is an attractive biomass feedstock due to its abundance. Traditionally, cassava is utilized as a foodstuff or for starch and bioethanol production. The price of cassava is determined by its starch content, while the remaining parts of the root, including the solid residue and peel, are often discarded, causing environmental problems. Utilizing the entire cassava plant can increase the economic benefits for farmers and significantly mitigate environmental issues (Simanjuntak et al., 2021). Rubber seed oil was chosen due to the availability of rubber seeds as a byproduct of rubber plantations. Rubber seeds are known to contain an oil content of up to 59%, but their utilization remains very limited (Pandiangan et al., 2016). A previous study by Simanjuntak et al., 2019, states that pyrolysis with a single raw material is not promising and tends to produce less yield. For this reason, by incorporating these two feedstocks, we aim to explore their potential as valuable resources, thereby promoting their uses and adding value to cassava and rubber plantations.

Previous studies have reported that zeolite-A synthesis has been conducted using various feedstocks, such as natural zeolite (Ginting et al., 2019), kaolin clay (Mendoza, 2017), fly ash (Andarini et al., 2018), rice husk silica (Simanjuntak et al., 2019), and a combination of rice husk silica and aluminum foil (Simanjuntak et al., 2021). Tatlier and Atalay-Oral (2016) reported that clinoptilolite-type natural zeolite was transformed into zeolite-A using an aluminum solution in an alkaline solvent. Thus, our study offers a novel approach by utilizing Lampung natural zeolite (LNZ), which has not been widely explored, and mixing a cassava and rubber seed oil on producing bio-crude oil with a high hydrocarbon content. Specifically, our study investigated the transformation prospects of clinoptilolite-type natural zeolite from Lampung (LNZ) into zeolite-A by adjusting the aluminum content to achieve Si/Al ratios of 1.0, 1.5, and 2.0. The resulting zeolites were subsequently utilized as catalysts in the pyrolysis process of a mixture of cassava and rubber seed oil. The objective was to determine the optimal Si/Al ratio for producing zeolite-A and to examine the correlations between the zeolite's Si/Al ratio and the yield and composition of the produced BCO, with a particular focus on the bio-hydrocarbon content. As a contribution, our study promotes the use of underutilized biomass resources, potentially offering an environmentally friendly and economically viable alternative for bio-oil production.

2. Methods

2.1 Materials and Instruments

We used the following materials: a Merck-produced reagent-grade sodium hydroxide, food-grade aluminum foil (FGAF), cassava tubers, and clinoptilolite-type Lampung Natural Zeolite (LNZ). Prior to use, LNZ was washed and soaked in distilled water for 24 hours. The sample was then dried for 24 hours at 100 °C and subsequently ground into a 200-mesh powder. Rubber seed oil was mechanically extracted using a DL-ZYJ02 oil press machine (Pandiangan et al., 2016). The laboratory instruments used included:

- A polytetrafluoroethylene (PTFE) lined stainless steel autoclave for the crystallization process,
- A PANalytical Epsilon 3 for X-ray fluorescence (XRF) analysis,
- A PANalytical Empyrean diffractometer for X-ray diffraction (XRD), and
- A ZEISS EVO MA 10 scanning electron microscope (SEM) for material characterization.
- BCO was produced using a laboratory-scale pyrolysis unit and analyzed using a GCMS-QP2010S SHIMADZU gas chromatography-mass spectrometry system.

A comprehensive analysis of raw materials in this study, which are cassava and rubber seed oil, refers to the previous studies by Simanjuntak et al. (2019) and Pandiangan et al. (2016).

2.2 Zeolite Transformation

Zeolite-A was prepared according to the required Si/Al ratio adjustments. Ratio adjustments for Si/Al were obtained through the calculations that can be seen in Appendix 1. The transformation of LNZ involved dissolving the necessary amount of FGAF in 250 ml of 1 M NaOH. Then, 50 g of LNZ was added to the solution, followed by the addition of 100 ml of distilled water. The mixture was aged for 24 hours in an autoclave at room temperature and subsequently subjected to crystallization at 100 °C for 72 hours. The resulting sample was washed, filtered, and dried for 8 hours at 80 °C, and then calcined for 6 hours at 550 °C. The sample was then ground into a powder and sieved using a 325-mesh screen. As a control, LNZ, without any composition adjustment, was also subjected to the same calcination treatment.

2.3 Zeolite Characterization

The transformation of natural zeolite requires adjusting the Si/Al ratio. To achieve this, XRF analysis was conducted to determine the composition of LNZ and obtain its Si/Al ratio as a basis for composition adjustment. The analysis was performed using a PANalytical Epsilon 3 XRF spectrometer, operating at a voltage of 30 kV, a current of 300 μA, and an input count rate of 13352.2 cps.

To analyze the transformed zeolites, the structure and surface morphology of the samples were evaluated using XRD and SEM techniques. The XRD patterns were identified using a PANalytical diffractometer with a Cu anode material, operating at 40 kV energy and 30 mA current, with a diffraction angle (2θ) range of 5–50°. Data obtained were analyzed using Match!3 software (Ver. 2.4.7 build 529) and compared to the standard data available in the International Zeolite Association (IZA) database. The surface morphology was examined using a ZEISS EVO MA 10 SEM, with an electron acceleration voltage of 15.00 kV, a window (WD) of 8.5 to 9.5 mm, and magnification (Mag) up to 35,000 times.

2.4 Catalytic Activity Test

The pyrolysis experiment was conducted under ambient conditions in a laboratory-scale pyrolysis unit with a steel tube reactor. The feedstock, consisting of a mixture of 100 g of cassava and 300 ml of rubber seed oil, was mixed with 10 g of catalyst and then transferred into the pyrolysis unit. The peak

temperature for pyrolysis was set at 350 °C by heating the reactor until it was reached and allowed to proceed for 90 minutes.

After pyrolysis, the liquid product was transferred into a separatory funnel to separate the water phase from the organic phase (BCO). The organic phase was then analyzed using a GCMS-QP2010SE SHIMADZU gas chromatography-mass spectrometry system. The analysis utilized an Rtx 5 column with the following specifications: 30 m length, 0.25 mm internal diameter (ID), and 0.25 µm film thickness. Helium was used as the carrier gas, with an electron ionization (EI) energy of 70 eV. The injector temperature was set to 310 °C with split mode operation. The detector temperature was 250 °C, and the oven column temperature was initially set at 40 °C. The flow rate was maintained at a pressure of 13 kPa, with a total flow rate of 80 ml/min.

3. Results and Discussions

3.1 Lampung Natural Zeolite Characterization

To determine the elemental and oxide composition of the natural zeolite used, the sample was characterized using XRF (X-ray fluorescence) analysis. The data obtained are presented in Table 1. Based on the results of the XRF analysis, aluminum and silicon were identified as the main components of the zeolite, with other components present in relative percentages ranging from 0.214% to 5.311%, resulting in an overall Si/Al ratio of 6.4.

Table 1. Elemental and oxide composition of natural zeolite.

No	Element	Relative percentage (%)	Oxide	Relative percentage (%)
1	Si	72.937	SiO_2	78.652
2	Al	10.941	Al_2O_3	12.744
3	K	5.311	K_2O	2.442
4	Ca	4.726	CaO	2.404
5	Fe	3.340	Fe_2O_3	1.624

XRD characterization was conducted to study the phases of LNZ, and the pattern was analyzed using Match!3 software, version 2.4.7 build 529. The diffractogram (Figure 1a) shows that the positions (2θ) of the diffraction peaks of the samples are in agreement with those for clinoptilolite and mordenite, as available in the Match!3 databases. This confirms the existence of clinoptilolite as the prominent phase and mordenite as a minor phase. Regarding relative intensities, varying values are observed between the corresponding peaks in the sample and those in the Match!3 database. This discrepancy is likely attributed to the presence of an amorphous phase in the sample, whereas the standard data originate from a pure crystalline phase. To obtain some insight on surface morphology, the LNZ sample was characterized using SEM, and the micrograph produced can be seen in Figure 2.

An additional examination involved comparing the XRD data of LNZ with the records in the International Zeolite Association (IZA) database for clinoptilolite (Framework Code HEU). The outcome of this comparison is illustrated in Figure 1b. As shown, the diffractogram of LNZ exhibits a similar pattern to that of the IZA standard for clinoptilolite, although the evident existence of an amorphous phase in the sample should also be acknowledged. Based on this agreement, the presence of clinoptilolite in LNZ is confirmed.

To gain further insight into the surface morphology, the LNZ sample was characterized using SEM. The micrograph of the sample in Figure 2 clearly indicates the heterogeneous characteristics of the surface, marked by particles of different shapes and sizes. Additionally, the micrograph displays irregular forms, most likely associated with the amorphous phase in the sample, as also indicated by the XRD diffractogram.

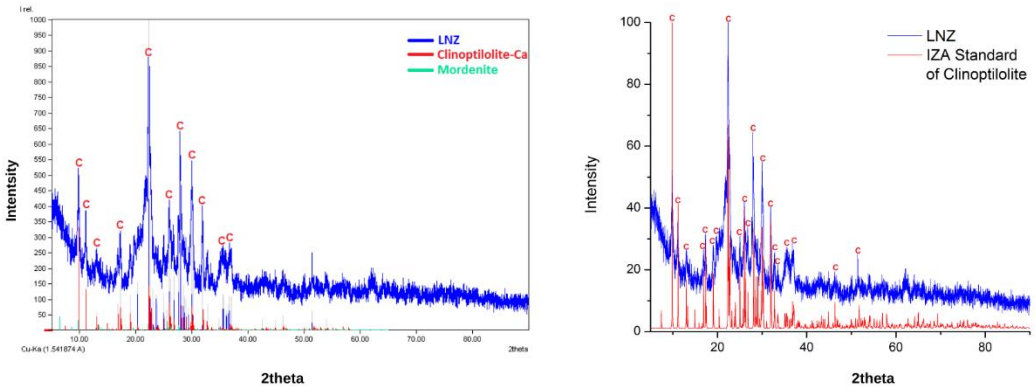

(a) (b)

Figure 1. Diffractogram of LNZ and the phases identified using Match!3 (a) and compared to IZA Database – Framework HEU (b).

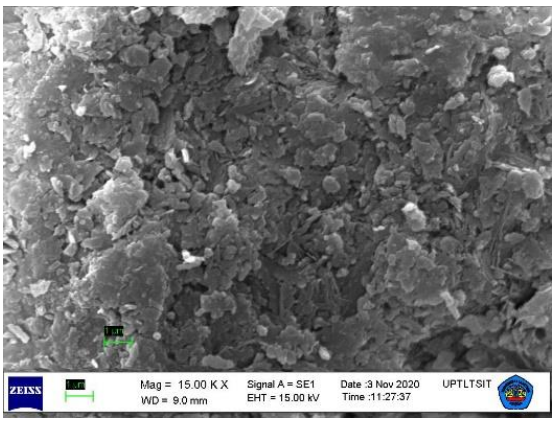

Figure 2. Micrograph of LNZ (Magnification 15,000x).

3.2.1 Transformation of Lampung Natural Zeolite

The XRD diffractograms of the four samples are compiled in Figure 3. The first feature that can be observed is a significant increase in the crystallinity of the samples compared to the original LNZ sample without treatment. The XRD patterns clearly indicate that the Zeo-C and Zeo-R2 samples are composed of zeolite-P as a prominent phase, according to Match!3 databases (Figures 3a and 3b). However, the existence of an amorphous phase is also evident.

Subsequent analysis involved comparing the XRD data of LNZ with the data available in the International Zeolite Association (IZA) database for zeolite-P (framework GIS), revealing a convincing resemblance between the patterns. The positions (2θ) and relative intensities of the observed peaks in the sample were then compared with those in the IZA standard, and the results are presented in Table 2. The data presented in Table 2 indicates satisfactory agreement between the samples and the standard from the IZA database. As shown, the five main peaks observed in the samples correspond with the characteristic peaks of zeolite-P.

Table 2. The comparison of IZA standard of Zeolite-P, Zeo-C and Zeo-R2 data.

IZA Standard of Zeolite-P		**Zeo-C**		**Zeo-R2**	
2θ	**Intensity (%)**	**2θ**	**Intensity (%)**	**2θ**	**Intensity (%)**
12.45	79.73	12.37	85.82	12.35	57.67
17.64	57.97	17.58	37.95	17.56	30.93
21.65	64.15	21.56	77.17	21.59	66.30
28.07	100	28.09	100	27.95	100
33.35	44.31	33.31	51.25	33.31	47.82

The transformation indicated by a significant phase change occurs from natural zeolite, specifically clinoptilolite, to zeolite-P. Active Al and Si species are formed by adding NaOH to natural zeolite. These species often react with one another and recombine to produce ring-like structures that serve as the basic formation of zeolites (Meor et al., 2006). According to Hong and Um (2021), the NaOH solution can successfully transform natural zeolite into Na-P zeolite through contact areas on the surface. The results also show that an ionic exchange occurs between Ca^{2+} and Na^{+}, as evidenced by Match!3 results, where the phase formed is identified as zeolite-P type Na-P_1. In terms of the Si/Al ratio, zeolite-P has various ratios. Previous studies have reported that zeolite-P can be synthesized with ratios of 1.75 (Hong & Um, 2021), 2.0–7.5 (Meor et al., 2006), 3.0–6.0 (Huo et al., 2012), and 3.0–15 (Azizi et al., 2013). Therefore, even without aluminum addition, the Si/Al ratio of LNZ falls within the range of zeolite-P ratios.

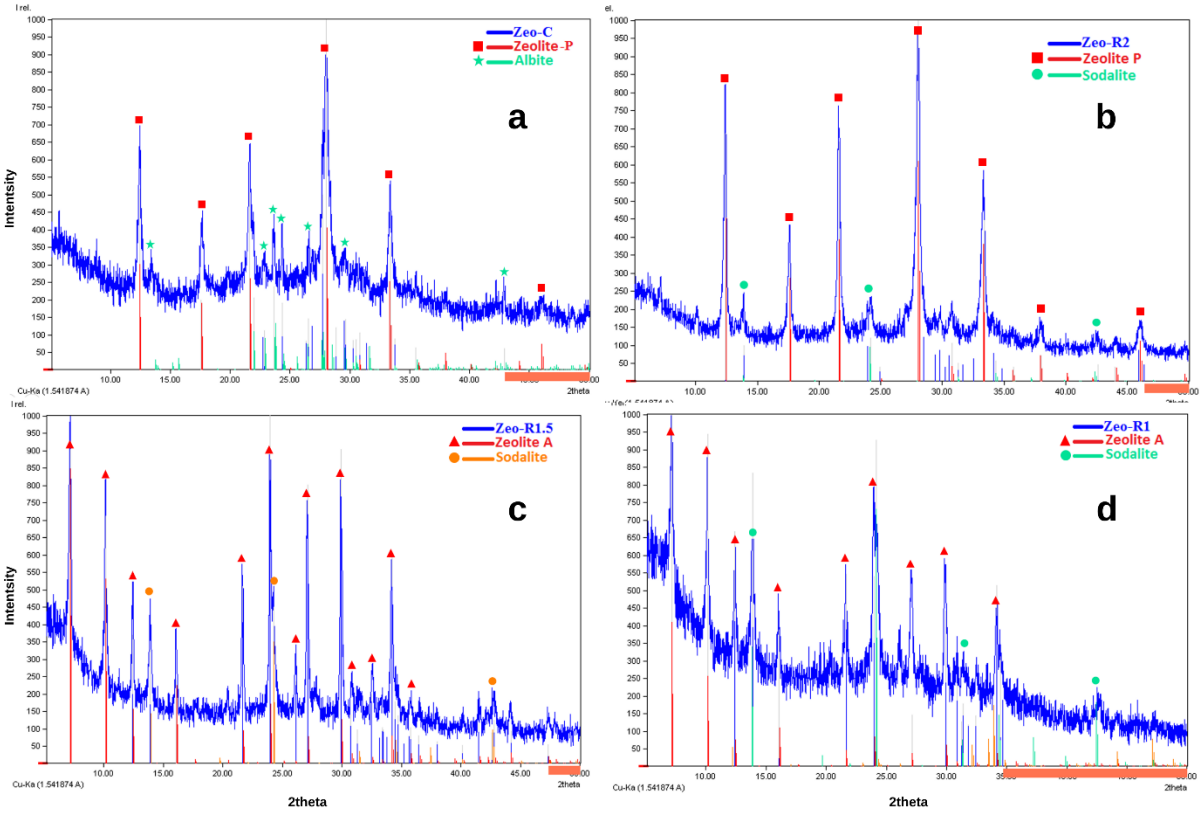

Figure 3. The XRD pattern of Zeo-C (a); Zeo-R2 (b); Zeo-R1.5 (c); and Zeo-R1 (d).

Zeo-R2, which has an adjusted Si/Al ratio of 2.0 (Figure 3b), has zeolite-P as the main phase and sodalite as the secondary phase. Regarding relative intensities, Zeo-R2 exhibits higher intensity and greater crystallinity than Zeo-C after the addition of FGAF. Consistent with previous results, a good agreement between the experimental data and the IZA standard was also observed for Zeo-R2, as shown in Table 2, justifying the formation of zeolite-P. There is no significant phase change from Zeo-C to Zeo-R2, as both transform into zeolite-P. However, the amount of aluminum added makes Zeo-R2 more crystalline than Zeo-C. Additionally, the secondary phase formed in Zeo-R2 was sodalite instead of albite found in Zeo-C.

The diffractograms of Zeo-R1.5 and Zeo-R1 in Figures 1c and 1d show different patterns compared to the previous samples (Zeo-C and Zeo-R2). The most distinctive difference is the formation of zeolite-A, indicating that the transformation of natural zeolite into zeolite-A was successfully achieved using the proposed method.

According to the Match!3 analysis results shown in Figures 3c and 3d, the main phase in the samples is zeolite-A, with sodalite as the secondary phase. The comparison with the IZA data for the zeolite-A

standard (framework LTA), as presented in Table 3, provides further evidence of the successful formation of zeolite-A. Zeo-R1.5 and Zeo-R1 both exhibit seven peaks that are recognized as prominent peaks of zeolite-A, confirming their transformation into zeolite-A. However, the evident existence of an amorphous phase in the samples should also be acknowledged. The successful transformation indicates a significant phase change from Zeo-C to Zeo-R1.5. Compared to Zeo-R1.5, the results show that Zeo-R1 contains a higher amorphous phase.

Table 3. The comparison of IZA standard of Zeolite-A, Zeo-R1.5 and Zeo-R1 data.

IZA Standard of Zeolite-A		Zeo-R1.5		Zeo-R1	
2θ	**Intensity (%)**	**2θ**	**Intensity (%)**	**2θ**	**Intensity (%)**
7.17	100	7.09	93.17	6.98	86.87
10.15	51.31	10.05	88.11	10.00	74.23
12.44	31.82	12.34	53.01	12.29	40.81
23.96	44.34	23.83	100	23.77	100
27.09	41.01	26.98	61.50	26.91	79.37
29.91	19.92	29.78	62.85	29.73	83.33
34.14	27.06	34.07	39.36	33.98	58.37

3.2.2 Surface Morphology Characterization

The morphology of zeolite-P has been widely reported in previous studies. Hong and Um (2021) noted that zeolite-P forms spherical clusters consisting of various bulkier nanostructures of different sizes, including square bipyramids (Figure 4a). The micrograph of Zeo-C in Figure 4b shows square bipyramid crystals (red circle), while albite morphology is indicated (yellow circle).

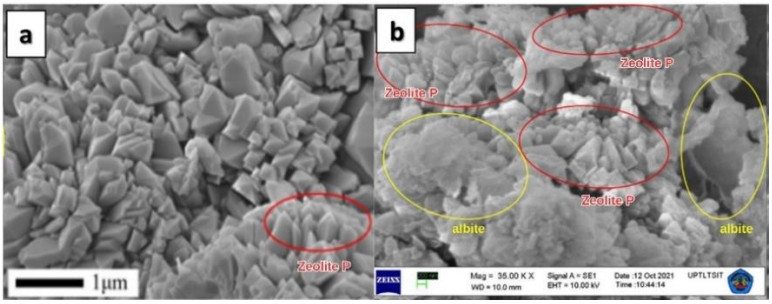

Figure 4. Micrograph of zeolite-P reported by Hong and Um (2021) (a), and micrograph of Zeo-C (b).

In contrast, the micrograph of Zeo-R2 in Figure 5a, at a magnification of 15,000x, shows that the crystals are more dispersed than the particles in Zeo-C. Increasing the magnification to 35,000x enhances the visibility of square bipyramid crystals of zeolite-P (red circle in Figure 5b) and sodalite (yellow circle). These results are consistent with the XRD data, although the presence of an amorphous phase is also acknowledged, contributing to the imperfect shape of the zeolite-P crystals.

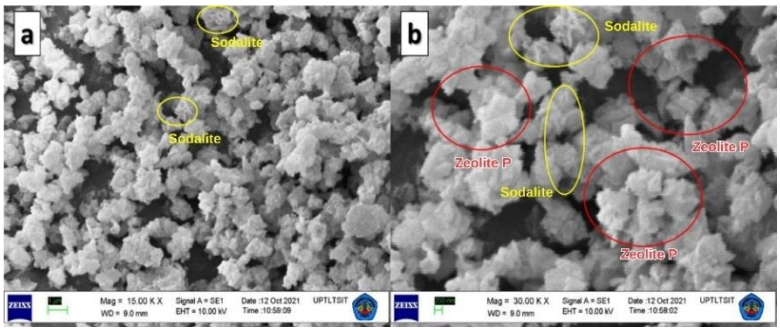

Figure 5. Micrograph of Zeo-R2 magnification of 15,000 x (a), and magnification of 35,000 x (b).

The micrograph of Zeo-R1.5 in Figure 6 clearly shows the cubic crystal structure, a characteristic feature of zeolite-A, as reported by Simanjuntak et al. (2021). It is also observed that some of the crystals have formed agglomerates. Sodalite as a secondary phase is indicated by rod-like structures on the surface of the sample. Compared with Zeo-R1.5, the micrograph of Zeo-R1 (Figure 7), at different magnifications, displays more evident agglomeration of the particles and smaller particle sizes. Additionally, the sample appears to be more amorphous and porous.

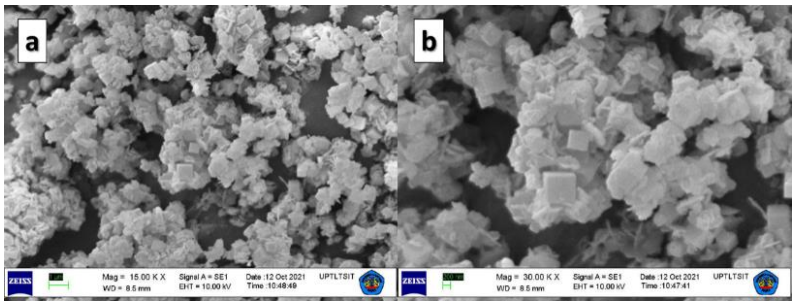

Figure 6. Micrograph of Zeo-R1.5 Magnification of 15,000 x (a), and Magnification of 30,000 x (b).

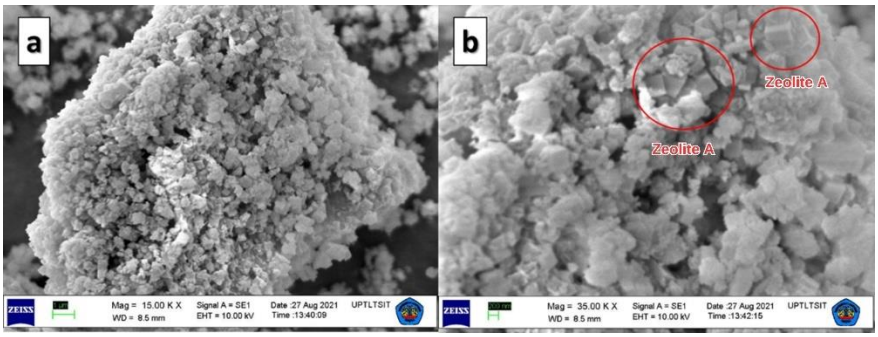

Figure 7. Micrograph of ZA-R1 Magnification of 15,000 x (a), and Magnification of 35,000 x (b).

3.3 Catalytic Activity Test

The GC chromatograms of the BCO produced from the pyrolysis experiment carried out without a catalyst are presented in Figure 8. Numerous peaks are distributed across the retention time from 2.0 to 43.49 minutes. This profile indicates that the sample is composed of various chemical components with different molecular weights and structures.

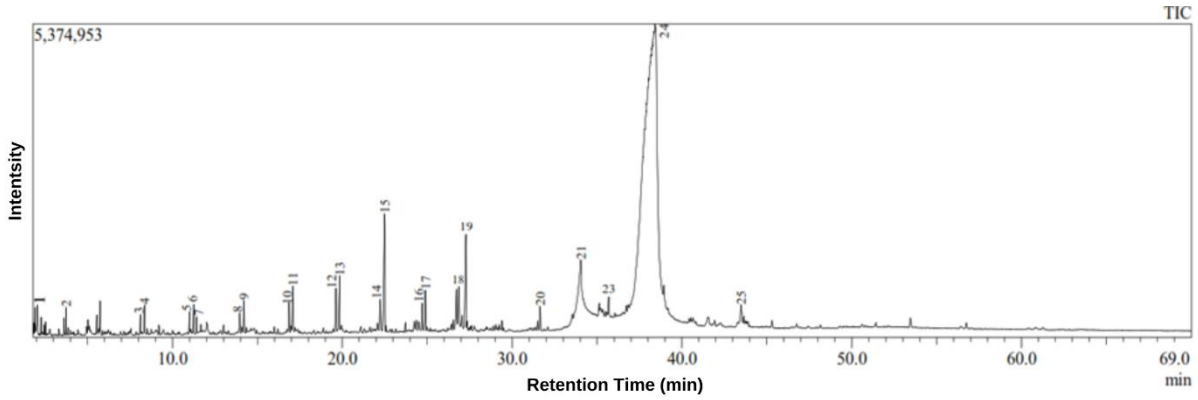

Figure 8. GC chromatogram of BCO obtained without catalyst.

In the chromatogram, many peaks have very low intensities and were therefore not identified. Each peak represents a different component, with varying peak areas indicating the relative percentages associated with each component. Using the WILEY7.LIB library system, 25 peaks were identified, as

shown in Figure 8 and presented in Table 4. The relative percentages in Table 4 were calculated using the following formula:

$$\% \, i = \frac{A_i}{A_t} \times 100 \quad (1)$$

where:
% i = relative percentage of component i
A_i = peak area of component i
A_t = total peak area of all identified components

To facilitate a more effective interpretation of the data, the 25 identified compounds were classified into several general chemical classes. By classifying the BCO components and specifying the composition in terms of the relative percentages of these classes, it becomes possible to compare BCO produced with various catalysts, given the observed variation in components. The relative composition of BCO produced from the experiment without a catalyst, using this grouping method, is presented in Figure 9.

Table 4. Chemical compounds of BCO produced from experiment without catalyst.

Peak No.	Retention Time (min)	Compounds	Formula	Relative Percentage (%)	Category
1	2.05	2,3-dimethyl-1-Pentanol	$C_7H_{16}O$	0.59	Alcohol
2	3.74	Octane	C_8H_{18}	0.32	Hydrocarbon
3	8.11	1-Decene	$C_{10}H_{20}$	0.27	Hydrocarbon
4	8.35	Decane	$C_{10}H_{22}$	0.42	Hydrocarbon
5	11.00	1-Undecene	$C_{11}H_{22}$	0.40	Hydrocarbon
6	11.25	Dodecane	$C_{12}H_{26}$	0.53	Hydrocarbon
7	11.42	(E)-4-Undecene	$C_{11}H_{22}$	0.29	Hydrocarbon
8	13.96	1-Dodecene	$C_{12}H_{24}$	0.32	Hydrocarbon
9	14.21	Tridecane	$C_{13}H_{28}$	0.60	Hydrocarbon
10	16.86	(Z)-3-Tetradecene	$C_{14}H_{28}$	0.56	Hydrocarbon
11	17.09	Hexadecane	$C_{16}H_{34}$	0.94	Hydrocarbon
12	19.63	1-Pentadecene	$C_{15}H_{30}$	0.93	Hydrocarbon
13	19.85	Isohexadecane	$C_{16}H_{34}$	1.31	Hydrocarbon
14	22.24	1-Heptadecene	$C_{17}H_{34}$	0.79	Hydrocarbon
15	22.50	Pentadecane	$C_{15}H_{32}$	3.91	Hydrocarbon
16	24.71	(E)-3-Octadecene	$C_{18}H_{36}$	0.62	Hydrocarbon
17	24.89	Eicosane	$C_{20}H_{42}$	0.88	Hydrocarbon
18	26.72	Heptadec-8-ene	$C_{17}H_{34}$	1.28	Hydrocarbon
19	26.87	(E)-9-Octadecene	$C_{18}H_{36}$	1.40	Hydrocarbon
20	27.28	2-Heptadecane	$C_{17}H_{36}$	2.88	Hydrocarbon
21	31.65	Heptadecanone	$C_{17}H_{34}O$	0.54	Ketone
22	34.05	2-Hexadecanoic acid	$C_{16}H_{32}O_2$	3.70	Carboxylic acid
23	35.68	9,12-Hexadecanone	$C_{16}H_{32}O$	0.42	Ketone
24	38.33	Methyl ester Hexadecadienoic acid	$C_{17}H_{30}O_2$	75.42	Ester
25	43.49	3,12-diethyl-2,5,9-Tetradecatriene	$C_{18}H_{32}$	0.69	Hydrocarbon

The components were classified into five classes, with esters dominating and contributing up to 75%. Although 20 out of the 25 compounds found are hydrocarbons, their contribution to the relative composition is only around 19%. This indicates that pyrolysis without a catalyst failed to create usable BCO as a potential fuel as methyl ester, the main component of rubber seed oil, still dominates. The BCO obtained using the remaining catalysts was processed in the same way, and the results obtained with all four catalysts are collected in Figure 10.

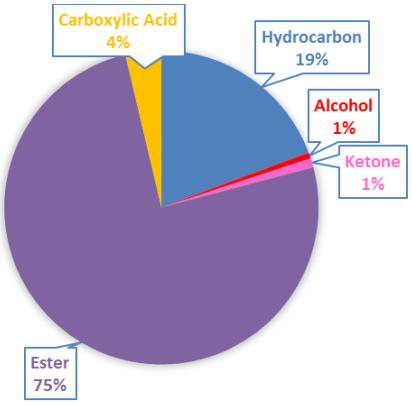

Figure 9. Relative compositions of BCO obtained without catalyst.

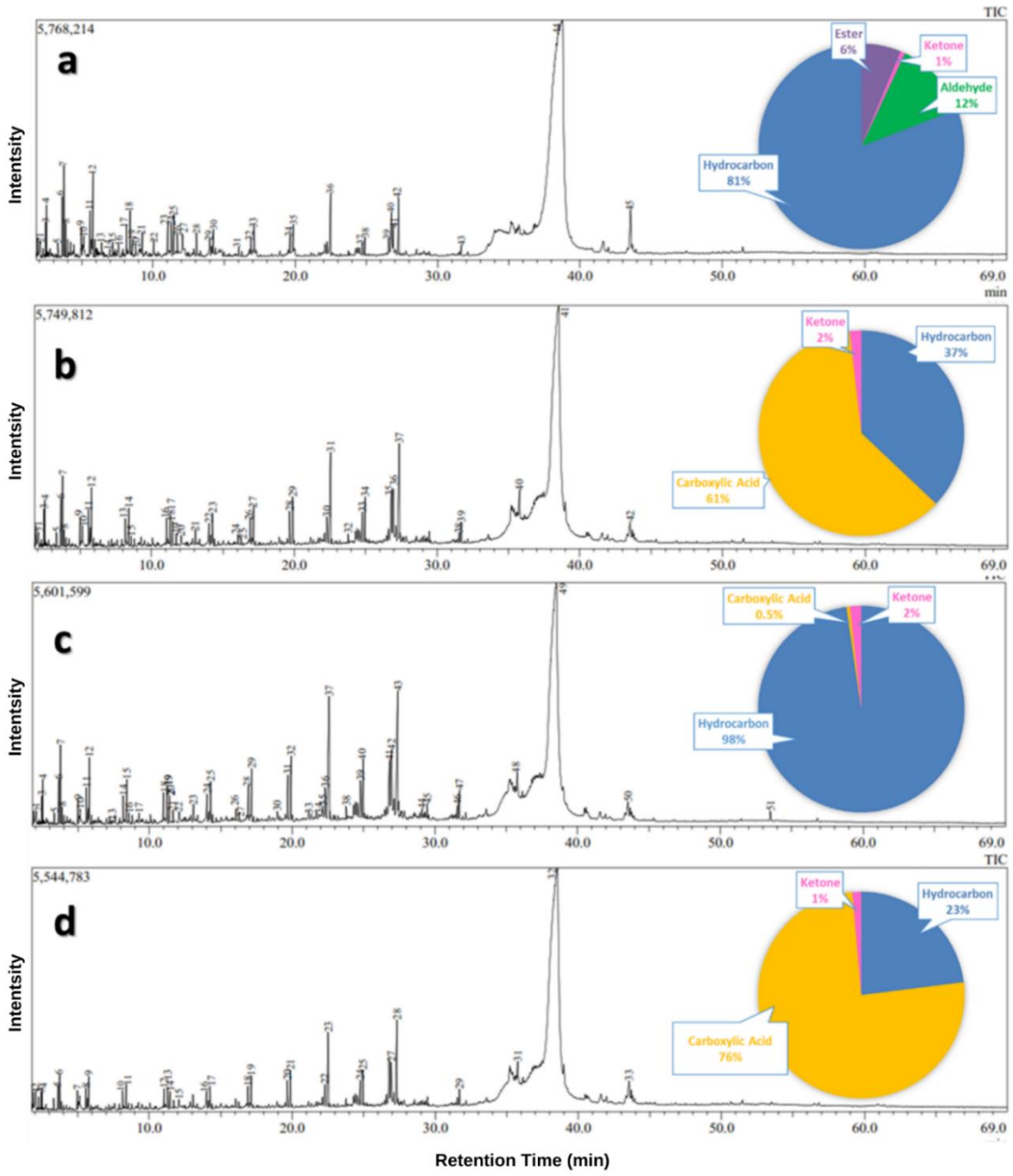

Figure 10. GC-Chromatograms and relative compositions of BCO obtained using transformed zeolites as catalyst Zeo-C (a), Zeo-R2 (b), Zeo-R1.5 (c), and Zeo-R1 (d).

The chromatograms of the samples shown in Figure 10 are generally similar, confirming the formation of the same compounds in the BCO, although some differences are observed. Compared to the results obtained without a catalyst, the diagram in Figure 10a indicates a sharp decrease in esters and a significant increase in hydrocarbons. This suggests that treating natural zeolite with NaOH improves the selectivity of zeolite for the formation of hydrocarbons. The addition of FGAF in the catalyst reduced the presence of esters and aldehydes but led to a high acid content, except in Zeo-R1.5. These results indicate that the Zeo-R1.5 catalyst, with a Si/Al ratio of 1.5, had the optimum performance in terms of hydrocarbon formation. A full analysis of each component for each catalyst can be seen in the Appendix.

The pyrolysis of a mixture of 100 g of cassava and 300 ml of rubber seed oil, using the transformed zeolites as catalysts, resulted in the production of bio-oil. Specifically, the conversion yielded 100 ml of bio-oil from the mixture, demonstrating the efficiency of the catalytic process. The BCO produced by using Zeo-C and Zeo-R1.5 as catalysts has the highest hydrocarbon content of 81% and 98%, respectively.

4. Conclusions

Our study presents an innovative approach by leveraging LNZ, a relatively untapped resource, in conjunction with a blend of cassava and rubber seed oil to produce BCO with a high hydrocarbon content. This method explores the catalytic potential of LNZ, which has not been widely studied, and the synergy of using these specific biomass oils, aiming to enhance the efficiency and quality of BCO production. The experimental results demonstrate that Lampung natural zeolite (LNZ) has been successfully transformed into zeolite-A by adjusting the Si/Al ratios to 1.5 and 1.0 from the original ratio of 6.4, using FGAF addition. The catalytic conversion yielded 100 ml of bio-oil from the mixture of cassava and rubber seed oil. The results of the pyrolysis experiments revealed that transforming LNZ to zeolite-A (Zeo-R1.5) led to a significant improvement in performance in terms of bio-hydrocarbon production. This is reflected by the increase in bio-hydrocarbon content from 81% in the BCO using Zeo-C to 98% with the use of Zeo-R1.5.

Our study makes a valuable contribution by advocating for the utilization of underexplored biomass resources, which are often overlooked. By tapping into these abundant yet underutilized materials, our approach aims to offer a sustainable and cost-effective solution for bio-oil production. This not only supports the development of greener energy alternatives but also enhances the economic viability of bio-oil, potentially reducing dependence on traditional fossil fuels and contributing to a more sustainable energy landscape.

Acknowledgments

The authors acknowledge the Department of Chemistry, Faculty of Mathematics and Natural Science, University of Lampung, for laboratory facilities support. The authors also acknowledged the Integrated Laboratory and Center for Technology Innovation, University of Lampung, for technical assistance.

References

Andarini, N., Lutfia, Z., & Haryati, T. (2018). Sintesis zeolit A dari abu terbang (fly ash) batubara variasi rasio molar Si/Al. *Jurnal Ilmu Dasar, 19*(2), 105–110. https://doi.org/10.19184/jid.v19i2.5910

Azizi, S. N., Daghigh, A. A., & Abrishamkar, M. (2013). Phase transformation of zeolite P to Y and analcime zeolites due to changing the time and temperature. *Journal of Spectroscopy*. https://doi.org/10.1155/2013/428216

Dewan Energi Nasional. (2019). *Outlook Energi Indonesia*. Sekretariat Jenderal Dewan Energi Nasional.

Ginting, S. Br., Perdana, G. A., Darmansyah, Iryani, D. A., & Wardono. (2019). Pengaruh waktu aging pada sintesis zeolit Linde Type-A (LTA) dari zeolit alam Lampung (ZAL) dengan metode step

change temperature of hydrothermal. *Jurnal Rekayasa Kimia dan Lingkungan, 14*(1), 1–11. https://doi.org/10.23955/rkl.v14i1.12093

Hong, S., & Um, W. (2021). Top-down synthesis of NaP zeolite from natural zeolite for the higher removal efficiency of Cs, Sr, and Ni. *Minerals, 11*(3). 252. https://doi.org/10.3390/min11030252

Huo, Z., Xu, X., Lü, Z., Song, J., He, M., Li, Z., Wang, Q., & Yan, L. (2012). Synthesis of zeolite NaP with controllable morphologies. *Microporous and Mesoporous Materials, 158*. 137–140. https://doi.org/10.1016/j.micromeso.2012.03.026

Iryani, D. A., Kumagai, S., Nonaka, M., Sasaki, K & Hirajima, T. (2017). Characterization and production of solid biofuel from sugarcane bagasse by hydrothermal carbonization. *Waste and Biomass Valorization, 8*(6). 1941–1951. https://doi.org/10.1007/s12649-017-9898-9

Kristianingrum, M. A., Gunawan, R., & Kartika, R. (2016). Pengaruh variasi rasio Si/Al struktur zeolit A dan variasi kation (Li^+, Na^+, K^+) terhadap perubahan ukuran *window* zeolit A menggunakan metode mekanika molekuler. *Jurnal Kimia Mulawarman, 14*(1). 46–53.

Mendoza, J. G. G. (2017). *Synthesis and applications of low silica zeolites from Bolivian clay and diatomaceous earth*. Lulea University of Technology.

Meor, M. S. Y., Muslim, M., Choo, T. F., & Murshidi, J. A. (2006). High purity alumina and zeolite from local low grade kaolin. *Proceedings of the 1st International Conference on Natural Resources Engineering & Technology 2006 Putrajaya, Malaysia*. 471–478.

Ngapa, Y. D., Sugiarti, S., & Abidin, Z. (2016). Hydrothermal transformation of natural zeolite from Ende-NTT and its application as adsorbent of cationic dye. *Indonesian Journal of Chemistry, 16*(2). 138–143. https://doi.org/10.22146/ijc.21156

Pandiangan, K. D., Jamarun, N., Arief, S., Simanjuntak, W., & Rilyanti, M. (2016). The effect of calcination temperatures on the activity of CaO and CaO/SiO_2 heterogeneous catalyst for transesterification of rubber seed oil in the presence of coconut oil as a co-reactant. *Oriental Journal of Chemistry, 32*(6). 3021–3026. https://doi.org/10.13005/ojc/320622

Tatlier, M & Atalay-Oral, C. (2016). Crystallization of zeolite-A coatings from natural zeolite. *Material Research, 19*(6). 1469–1477. https://doi.org/10.1590/1980-5373-MR-2016-0564

Simanjuntak, W., Pandiangan, K. D., Sembiring, Z., & Simanjuntak, A. (2019). Liquid fuel production by zeolite-A catalyzed pyrolysis of mixed cassava solid waste and rubber seed oil. *Oriental Journal of Chemistry, 35*(1). 71–76. https://doi.org/10.13005/ojc/350108

Simanjuntak, W., Pandiangan, K. D., Sembiring, Z., & Sihombing, I. P. (2021). Biogasoline production by zeolite-A catalyzed co-pyrolysis of torrefied cassava root and palm oil. *Journal of Physics: Conference Series, 1751*. 012088. https://doi.org/10.1088/1742-6596/1751/1/012088

Supriyanto, R., Simanjuntak, W., Pandiangan, K. D., Situmeang, R. T. M., & Ahmadhani, M. Y. (2018). Chemical composition of liquid fuel produced by co-pyrolysis of sugarcane bagasse and sludge palm oil using zeolite-Y as catalyst. *Oriental Journal of Chemistry, 34*(3). 1533–1540. https://doi.org/10.13005/ojc/340345

Appendix

Appendix 1. The calculations of adjustment to Si/Al Ratio of zeolite-A

a. Si/Al Ratio of LNZ
   - Per 100 gram LNZ

$$\frac{Si/Ar_{Si}}{Al/Ar_{Al}} = \frac{72.937\ g/28\ g\ mol^{-1}}{10.941\ g/27\ \ g\ mol^{-1}} = \frac{2.6049}{0.4052} = 6.43$$

   - Per 50 gram LNZ

$$Si = \frac{72.937\ g}{2} = 36.4685\ g$$
$$n\ Si = \frac{36.4685\ g}{28\ g\ mol^{-1}} = 1.3024\ mol$$
$$Al = \frac{10.941\ g}{2} = 5.4705\ g$$
$$n\ Al = \frac{5.4705\ g}{27\ g\ mol^{-1}} = 0.2026\ mol$$
$$\frac{Si/Ar_{Si}}{Al/Ar_{Al}} = \frac{1.3024\ mol}{0.2026\ mol} = 6.43$$

b. Adjustment of Si/Al Ratio 2

$$n\frac{Si}{Al} = 2$$
$$\frac{1.3024\ mol}{n\ Al} = 2$$
$$n\ Al = \frac{1.3024\ mol}{2} = 0.6512\ mol$$
$$m\ Al = 0.6512\ mol\ x\ 27g\ mol^{-1} = 17.5824\ g$$

$$Aluminum\ addition = 17.5824\ g - 5.4705\ g = 12.1119\ g$$

c. Adjustment of Si/Al Ratio 1.5

$$n\frac{Si}{Al} = 1.5$$
$$\frac{1.3024\ mol}{n\ Al} = 1.5$$
$$n\ Al = \frac{1.3024\ mol}{1.5} = 0.8683\ mol$$
$$m\ Al = 0.8683\ mol\ x\ 27g\ mol^{-1} = 23.4441\ g$$

$$Aluminum\ addition = 23.4441\ g - 5.4705\ g = 17.9736\ g$$

d. Adjustment of Si/Al Ratio 1

$$n\frac{Si}{Al} = 1$$
$$\frac{1.3024\ mol}{n\ Al} = 1$$
$$n\ Al = \frac{1.3024\ mol}{1} = 1.3024\ mol$$
$$m\ Al = 1.3024\ mol\ x\ 27g\ mol^{-1} = 35.1648\ g$$

$$Aluminum\ addition = 35.1648\ g - 5.4705\ g = 29.6943\ g$$

Appendix 2. Chemical compounds of BCO produced from experiment using various catalysts.

Table A1. Chemical compounds of BCO produced using catalysts zeo-C.

Peak No.	Retention Time (min)	Compounds	Formula	Relative Percentage (%)	Category
1	1.901	Hexane	C_6H_{14}	0.62	Hydrocarbon
2	2.05	Methylcyclopentane	C_6H_{12}	1.88	Hydrocarbon
3	2.448	1-Heptene	C_7H_{14}	1.26	Hydrocarbon
4	2.516	Heptane	C_7H_{16}	1.79	Hydrocarbon
5	3.323	Methylbenzene	C_7H_8	0.89	Hydrocarbon
6	3.618	1-Octene	C_8H_{16}	3.04	Hydrocarbon
7	3.754	Octane	C_8H_{18}	4.44	Hydrocarbon
8	3.864	E-2-Octene	C_8H_{16}	1.35	Hydrocarbon
9	4.965	Ethylbenzene	C_8H_{10}	1.52	Hydrocarbon
10	5.134	1,3-Dimethylbenzene	C_8H_{10}	1.55	Hydrocarbon
11	5.565	1-Nonene	C_9H_{18}	2.73	Hydrocarbon
12	5.772	Nonane	C_9H_{20}	4.89	Hydrocarbon
13	6.389	(E)-1,3-Nonadiene	C_9H_{16}	0.77	Hydrocarbon
14	6.97	1-Butyl-2-ethylcyclopropene	C_9H_{16}	0.61	Hydrocarbon
15	7.167	Propylbenzene	C_9H_{12}	1.01	Hydrocarbon
16	7.58	4-Hexen-1-ylester-propinsaure	$C_9H_{16}O_2$	0.79	Ester
17	8.146	1-Decene	$C_{10}H_{20}$	1.68	Hydrocarbon
18	8.384	Decane	$C_{10}H_{22}$	2.93	Hydrocarbon
19	8.548	(Z)-2-Decene	$C_{10}H_{20}$	0.89	Hydrocarbon
20	8.775	(Z)-3-Decene	$C_{10}H_{20}$	0.54	Hydrocarbon
21	9.244	1-Limonene	$C_{10}H_{16}$	1.50	Hydrocarbon
22	10.053	Butylbenzene	$C_{10}H_{14}$	1.03	Hydrocarbon
23	11.041	1-Undecene	$C_{11}H_{22}$	2.19	Hydrocarbon
24	11.281	Tetradecane	$C_{14}H_{30}$	2.02	Hydrocarbon
25	11.466	(E)-4-Undecene	$C_{11}H_{22}$	2.64	Hydrocarbon
26	11.707	Octylcyclopropane	$C_{11}H_{22}$	1.21	Hydrocarbon
27	12.058	3-propyl-1,4-Pentadiene	C_8H_{14}	1.34	Hydrocarbon
28	13.060	Pentylbenzene	$C_{11}H_{16}$	2.02	Hydrocarbon
29	13.996	1-Dodecene	$C_{12}H_{24}$	1.10	Hydrocarbon
30	14.238	Dodecane	$C_{12}H_{26}$	1.69	Hydrocarbon
31	16.027	Hexylbenzene	$C_{12}H_{18}$	0.76	Hydrocarbon
32	16.878	1-Pentadecene	$C_{15}H_{30}$	1.05	Hydrocarbon
33	17.107	Tridecane	$C_{13}H_{28}$	2.16	Hydrocarbon
34	19.634	1-Tetradecene	$C_{14}H_{28}$	1.49	Hydrocarbon
35	19.846	Hexadecane	$C_{16}H_{34}$	2.44	Hydrocarbon
36	22.482	Pentadecane	$C_{15}H_{32}$	6.14	Hydrocarbon
37	24.713	1-Octadecene	$C_{18}H_{36}$	0.88	Hydrocarbon
38	24.887	Eicosane	$C_{20}H_{42}$	1.23	Hydrocarbon
39	26.566	5-Octadecyne	$C_{18}H_{34}$	1.30	Hydrocarbon
40	26.752	8-Heptadecene	$C_{17}H_{34}$	4.86	Hydrocarbon
41	26.875	(E)-9-Octadecene	$C_{18}H_{36}$	2.81	Hydrocarbon
42	27.265	Heptadecane	$C_{17}H_{36}$	4.64	Hydrocarbon
43	31.651	2-Heptadecanone	$C_{17}H_{34}O$	0.73	Ketone
44	38.458	(Z)-Octadecenal	$C_{18}H_{34}O$	12.16	Aldehyde
45	43.555	dioctyl ester-1,2-Benzenedicarboxylic acid	$C_{24}H_{38}O_4$	5.45	Ester

Table A2. Chemical compounds of BCO produced using catalyst zeo-R2.

Peak No.	Retention Time (min)	Compounds	Formula	Relative Percentage (%)	Category
1	1.907	Hexane	C_6H_{14}	0.32	Hydrocarbon
2	2.058	Acetic acid	$C_2H_4O_2$	0.52	Carboxylic acid
3	2.457	1-Heptene	C_7H_{14}	0.54	Hydrocarbon
4	2.526	Heptane	C_7H_{16}	0.67	Hydrocarbon
5	3.337	Methylbenzene	C_7H_8	0.34	Hydrocarbon
6	3.632	1-Octene	C_8H_{16}	0.85	Hydrocarbon
7	3.765	Octane	C_8H_{18}	1.20	Hydrocarbon
8	3.879	(E)-2-Octene	C_8H_{16}	0.28	Hydrocarbon
9	4.984	Ethylbenzene	C_8H_{10}	0.60	Hydrocarbon
10	5.157	1,3-dimethyl-Benzene	C_8H_{10}	0.71	Hydrocarbon
11	5.585	1-Nonene	C_9H_{18}	0.80	Hydrocarbon
12	5.783	Nonane	C_9H_{20}	1.27	Hydrocarbon
13	8.168	1-Decene	$C_{10}H_{20}$	0.61	Hydrocarbon
14	8.405	Decane	$C_{10}H_{22}$	1.01	Hydrocarbon
15	8.566	(Z)-2-Decene	$C_{10}H_{20}$	0.29	Hydrocarbon
16	11.062	1-Undecene	$C_{11}H_{22}$	0.70	Hydrocarbon
17	11.305	Tetradecane	$C_{14}H_{30}$	0.89	Hydrocarbon
18	11.478	(E)-4-Undecene	$C_{11}H_{22}$	0.59	Hydrocarbon
19	11.723	1-heptyl-2-methyl-Cyclopropane	$C_{11}H_{22}$	0.27	Hydrocarbon
20	12.076	3-propyl-1,4-Pentadiene	C_8H_{14}	0.39	Hydrocarbon
21	13.075	Pentylbenzene	$C_{11}H_{16}$	0.44	Hydrocarbon
22	14.024	(Z)-3-Tetradecene	$C_{14}H_{28}$	0.45	Hydrocarbon
23	14.267	Dodecane	$C_{12}H_{26}$	0.87	Hydrocarbon
24	16.058	hexyl-Benzene	$C_{12}H_{18}$	0.31	Hydrocarbon
25	16.275	(1,3-dimethylbutyl)-Benzene	$C_{12}H_{18}$	0.25	Hydrocarbon
26	16.915	1-Pentadecene	$C_{15}H_{30}$	0.67	Hydrocarbon
27	17.146	Tridecane	$C_{13}H_{28}$	1.09	Hydrocarbon
28	19.677	1-Tetradecene	$C_{14}H_{28}$	0.92	Hydrocarbon
29	19.894	Heptadecane	$C_{17}H_{36}$	1.42	Hydrocarbon
30	22.29	1-Heptadecene	$C_{17}H_{34}$	0.87	Hydrocarbon
31	22.542	Pentadecane	$C_{15}H_{32}$	3.97	Hydrocarbon
32	23.777	Undecyl-Cyclohexane	$C_{17}H_{34}$	0.26	Hydrocarbon
33	24.773	1-Octadecene	$C_{18}H_{36}$	1.00	Hydrocarbon
34	24.957	Hexadecane	$C_{16}H_{34}$	1.47	Hydrocarbon
35	26.803	8-Heptadecene	$C_{17}H_{34}$	2.48	Hydrocarbon
36	26.94	(E)-9-Octadecene	$C_{18}H_{36}$	2.50	Hydrocarbon
37	27.358	Eicosane	$C_{20}H_{42}$	4.68	Hydrocarbon
38	31.56	Tetracosane	$C_{24}H_{50}$	0.29	Hydrocarbon
39	31.705	2-Heptadecanone	$C_{17}H_{34}O$	0.65	Keton
40	35.776	2-Hexadecanone	$C_{16}H_{32}O$	1.17	Keton
41	38.525	(Z,Z)-9,12-Octadecadienoic acid	$C_{18}H_{32}O_2$	60.61	Carboxylic acid
42	43.534	5-Eicosyne	$C_{20}H_{38}$	0.81	Hydrocarbon

Table A3. Chemical compounds of BCO produced using catalyst zeo-R1.5.

Peak No.	Retention Time (min)	Compounds	Formula	Relative Percentage (%)	Category
1	1.903	Hexane	C_6H_{14}	0.22	Hydrocarbon
2	2.06	Acetic acid	$C_2H_4O_2$	0.54	Carboxylic acid
3	2.454	1-Heptene	C_7H_{14}	0.38	Hydrocarbon
4	2.523	Heptane	C_7H_{16}	0.51	Hydrocarbon
5	3.335	Methylbenzene	C_7H_8	0.24	Hydrocarbon
6	3.63	1-Octene	C_8H_{16}	0.65	Hydrocarbon
7	3.765	Octane	C_8H_{18}	1.09	Hydrocarbon
8	3.876	2-Octene	C_8H_{16}	0.22	Hydrocarbon
9	4.982	Ethylbenzene	C_8H_{10}	0.33	Hydrocarbon
10	5.153	1,3-dimethyl-Benzene	C_8H_{10}	0.29	Hydrocarbon
11	5.583	1-Nonene	C_9H_{18}	0.63	Hydrocarbon
12	5.786	Nonane	C_9H_{20}	1.25	Hydrocarbon
13	7.392	1,2,4-tris(methylene)-Cyclohexane	C_9H_{12}	0.26	Hydrocarbon
14	8.167	1-Decene	$C_{10}H_{20}$	0.50	Hydrocarbon
15	8.408	Decane	$C_{10}H_{22}$	0.93	Hydrocarbon
16	8.567	(Z)-2-Decene	$C_{10}H_{20}$	0.18	Hydrocarbon
17	9.263	1-Limonene	$C_{10}H_{16}$	0.24	Hydrocarbon
18	11.065	1-Undecene	$C_{11}H_{22}$	0.66	Hydrocarbon
19	11.313	Tetradecane	$C_{14}H_{30}$	0.93	Hydrocarbon
20	11.483	(E)-4-Undecene	$C_{11}H_{22}$	0.55	Hydrocarbon
21	11.728	1-heptyl-2-methyl-Cyclopropane	$C_{11}H_{22}$	0.26	Hydrocarbon
22	12.08	3-propyl-1,4-Pentadiene	C_8H_{14}	0.37	Hydrocarbon
23	13.081	Pentylbenzene	$C_{11}H_{22}$	0.37	Hydrocarbon
24	14.033	(Z)-3-Tetradecene	$C_{14}H_{28}$	0.52	Hydrocarbon
25	14.28	Tridecane	$C_{12}H_{24}$	0.97	Hydrocarbon
26	16.063	hexyl-Benzene	$C_{12}H_{18}$	0.34	Hydrocarbon
27	16.283	(1,3-dimethylbutyl)-Benzene	$C_{12}H_{18}$	0.29	Hydrocarbon
28	16.93	1-Pentadecene	$C_{15}H_{30}$	0.85	Hydrocarbon
29	17.164	Hexadecane	$C_{16}H_{34}$	1.34	Hydrocarbon
30	18.958	Heptyl-Benzene	$C_{13}H_{20}$	0.19	Hydrocarbon
31	19.695	1-Tetradecene	$C_{14}H_{28}$	1.27	Hydrocarbon
32	19.921	Heptadecane	$C_{17}H_{36}$	1.88	Hydrocarbon
33	21.164	decyl-Cyclopentane	$C_{15}H_{30}$	0.24	Hydrocarbon
34	21.85	2-Phenyl-3-Propyl-Hexan	$C_{15}H_{24}$	0.41	Hydrocarbon
35	22.14	(E)-7-Tetradecene	$C_{14}H_{28}$	0.58	Hydrocarbon
36	22.306	1-Heptadecene	$C_{17}H_{34}$	1.19	Hydrocarbon
37	22.589	Pentadecane	$C_{15}H_{32}$	5.74	Hydrocarbon
38	23.793	undecyl-Cyclohexane	$C_{17}H_{34}$	0.31	Hydrocarbon
39	24.791	(E)-3-Octadecene	$C_{18}H_{36}$	1.14	Hydrocarbon
40	24.981	Eicosane	$C_{20}H_{42}$	1.76	Hydrocarbon
41	26.818	8-Heptadecene	$C_{17}H_{34}$	2.65	Hydrocarbon
42	26.966	(E)-9-Octadecene	$C_{18}H_{36}$	3.13	Hydrocarbon
43	27.398	Octadecane	$C_{18}H_{38}$	6.13	Hydrocarbon
44	29.098	1-Nonadecene	$C_{19}H_{38}$	0.25	Hydrocarbon
45	29.466	Nonadecane	$C_{19}H_{40}$	0.39	Hydrocarbon
46	31.57	Tetracosane	$C_{24}H_{50}$	0.35	Hydrocarbon
47	31.716	2-Heptadecanone	$C_{17}H_{34}O$	0.82	Ketone

48	35.776	2-Hexadecanone	$C_{16}H_{32}O$	0.65	Ketone
49	38.5	9-Eicosyne	$C_{20}H_{38}$	54.06	Hydrocarbon
50	43.532	3,12-diethyl-2,5,9-Tetradecatriene	$C_{18}H_{32}$	0.66	Hydrocarbon
51	53.508	16-Hentriacontanone	$C_{31}H_{62}O$	0.29	Ketone

Table A4. Chemical compounds of BCO produced using catalyst zeo-R1.

Peak No.	Retention Time (min)	Compounds	Formula	Relative Percentage (%)	Category
1	1.903	Hexane	C_6H_{14}	0.31	Hydrocarbon
2	2.058	Acetic acid	$C_2H_4O_2$	0.73	Carboxylic acid
3	2.453	1-Heptene	C_7H_{14}	0.34	Hydrocarbon
4	2.522	Heptane	C_7H_{16}	0.30	Hydrocarbon
5	3.625	1-Octene	C_8H_{16}	0.38	Hydrocarbon
6	3.756	Octane	C_8H_{18}	0.55	Hydrocarbon
7	4.978	Ethylbenzene	C_8H_{10}	0.33	Hydrocarbon
8	5.574	1-Nonene	C_9H_{18}	0.43	Hydrocarbon
9	5.769	Nonane	C_9H_{20}	0.65	Hydrocarbon
10	8.156	1-Decene	$C_{10}H_{20}$	0.37	Hydrocarbon
11	8.39	Decane	$C_{10}H_{22}$	0.60	Hydrocarbon
12	11.05	1-Undecene	$C_{11}H_{22}$	0.45	Hydrocarbon
13	11.292	Tetradecane	$C_{14}H_{30}$	0.57	Hydrocarbon
14	11.465	(E)-4-Undecene	$C_{11}H_{22}$	0.38	Hydrocarbon
15	12.072	3-Propyl-1,4-pentadiene	C_8H_{14}	0.31	Hydrocarbon
16	14.015	1-Dodecene	$C_{12}H_{24}$	0.30	Hydrocarbon
17	14.255	Tridecane	$C_{13}H_{28}$	0.58	Hydrocarbon
18	16.906	(Z)-3-Tetradecene	$C_{14}H_{28}$	0.46	Hydrocarbon
19	17.132	Dodecane	$C_{12}H_{26}$	0.76	Hydrocarbon
20	19.664	1-Pentadecene	$C_{15}H_{30}$	0.70	Hydrocarbon
21	19.878	Hexadecane	$C_{16}H_{34}$	1.00	Hydrocarbon
22	22.278	1-Heptadecene	$C_{17}H_{34}$	0.71	Hydrocarbon
23	22.517	Heptadecane	$C_{17}H_{36}$	2.83	Hydrocarbon
24	24.761	(E)-3-Octadecene	$C_{18}H_{36}$	0.76	Hydrocarbon
25	24.938	Pentadecane	$C_{15}H_{34}$	1.05	Hydrocarbon
26	26.784	8-Heptadecene	$C_{17}H_{34}$	1.91	Hydrocarbon
27	26.922	(E)-9-Octadecene	$C_{18}H_{36}$	1.80	Hydrocarbon
28	27.33	Eicosane	$C_{20}H_{42}$	3.31	Hydrocarbon
29	31.696	2-Heptadecanone	$C_{17}H_{34}O$	0.47	Ketone
30	35.204	2-propenyl decanoate	$C_{13}H_{24}O_2$	0.52	Carboxylic acid
31	35.764	2-hexadecanone	$C_{16}H_{32}O$	0.90	Ketone
32	38.539	(Z,Z)-9,12-Octadecadienoic acid	$C_{18}H_{32}O_2$	74.35	Carboxylic acid
33	43.544	3,12-diethyl-2,5,9-Tetradecatriene	$C_{18}H_{32}$	0.87	Hydrocarbon